CRDS modelling of deuterium release from co-deposited beryllium layers in temperature programmed and laser induced desorption experiments

D Matveev[1] ⬤, M Zlobinski[1] ⬤, G De Temmerman[2] ⬤, B Unterberg[1] and C Linsmeier[1] ⬤

[1] Forschungszentrum Jülich GmbH, Institut für Energie- und Klimaforschung—Plasmaphysik, D-52425 Jülich, Germany
[2] ITER Organization, Route de Vinon-sur-Verdon, CS 90 046, F-13067 St Paul Lez Durance Cedex, France

E-mail: d.matveev@fz-juelich.de

CrossMark

Abstract

Deuterium release from Be/D layers co-deposited using high power impulse magnetron sputtering (HiPIMS) is modelled with rate equations using the CRDS code under conditions of temperature programmed (TPD) and laser induced (LID) Desorption experiments. TPD results are simulated to fit D trapping parameters that are in turn applied to simulate the LID. TPD results are compared to equivalent results from JET-ILW and UCSD samples. HiPIMS samples show a different release behavior compared to UCSD and JET samples, release peaks at comparable heating rates are narrower and cannot be modelled using the same set of parameters. With a particular choice of diffusion-trapping parameters that reproduce the TPD peak positions, modelling of the LID efficiency results in a qualitative agreement with experimental observations. In particular, it is shown that a complete outgassing of low D content samples is not possible during laser heating unless the surface temperature exceeds the Be melting threshold.

(Some figures may appear in colour only in the online journal)

1. Introduction

It has been demonstrated in the JET tokamak with the ITER-like wall (ILW) that the global fuel inventory is dominated by co-deposition with beryllium, mainly in the inner divertor region [1]. A similar situation is expected in ITER [2]. Understanding the trapping of hydrogen isotopes in Be co-deposits is therefore important to predict the efficiency of tritium recovery methods (baking of plasma-facing components) and retention diagnostics such as laser induced desorption (LID) planned in ITER [3].

Temperature programmed desorption (TPD) analysis, also often referred as thermal desorption spectroscopy (TDS), of samples from JET-ILW and respective TMAP7 modelling [3–5] reveal similarities and differences in trapping and release characteristics as compared to UCSD laboratory samples from Baldwin et al [6]. JET samples demonstrate deuterium (D) release up to higher temperatures compared to UCSD samples, which must be associated with different deposition conditions, layer thickness and to a large extent presence of non-negligible fraction of impurities in JET co-deposits. The efficiency of LID in ITER was addressed by TMAP7 modelling by Temmerman et al [3] for JET-like co-deposited layers. A systematic experimental validation of the LID efficiency has been performed recently by Zlobinski et al [7, 8] on co-deposited Be/D layers with pre-defined thicknesses and D contents produced in laboratory by high power impulse magnetron sputtering (HiPIMS) technique [9] on the
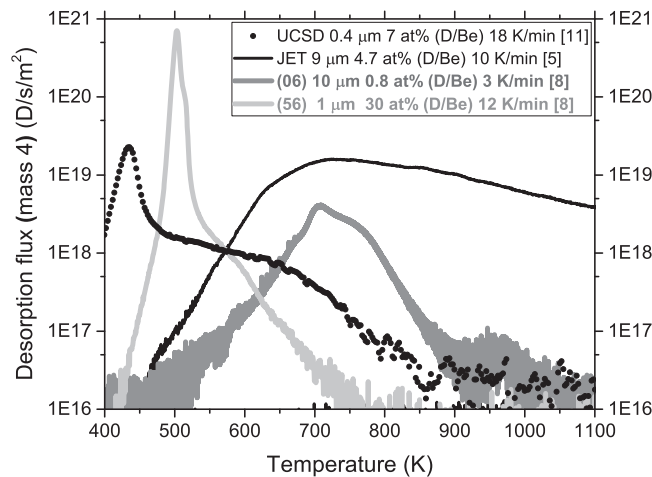
Figure 1. Measured TPD spectra of HiPIMS Be/D layers of different nominal thicknesses and D contents that were used for LID studies in [7] and [8]. For comparison two additional spectra are shown: one for the JET sample 1/10 from the upper part of the divertor Tile 1 exposed during the ILW-2 campaign [5] and one for a Be/D layer from UCSD [11] produced by a magnetron sputtering technique.

tungsten subsrate. TPD and nuclear reaction analyses (NRA) were performed to characterize the D content and release kinetics from the layers. The efficiency of LID as a function of the laser energy and pulse duration was assessed. Details of sample production and experimental procedure can be found elsewhere [7–9].

In this paper, we simulate the D release from such co-deposited layers with rate equations using the CRDS code [10]. TPD results are simulated to obtain D trapping parameters matching the experimental spectra. Selected parameters are then applied to simulate the LID process.

2. Modelling of temperature programmed desorption

Exemplary TPD spectra measured on HiPIMS samples of different nominal thicknesses and D contents that were used for LID studies in [7] and [8] are shown in figure 1 (sample 6: 10 μm layer, 0.8 at% D; sample 56: 1 μm layer, 30 at% D). For comparison the JET sample 1/10 from the upper part of the divertor Tile 1 exposed during the ILW-2 campaign is shown (9 μm layer, 4.7 at% D) [5] (figure 20(b) therein) together with a UCSD laboratory sample (0.4 μm layer, 7 at% D) produced by a magnetron sputtering technique [11] (figure 1 therein). The atomic fraction of D in the HiPIMS layers is calculated as the ratio of D atoms to Be atoms measured by NRA. The same is applied for the JET sample according to data given in table 1 in [5]. The thickness of the UCSD sample is as reported in [11], and the D content is recalculated from the time integral of the release flux. It has to be noted that measured atomic fraction of D in the 10 μm HiPIMS layer used for LID in [8] was about factor 2 higher than in the equivalent sample used for TDS (sample 3). This discrepancy may be attributed to different sample temperatures during deposition due to larger dimensions of LID samples compared to TDS samples. Apparent features of TPD
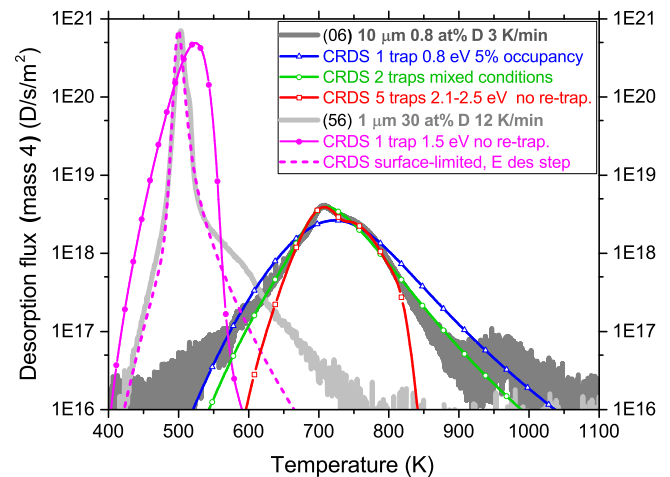

Figure 2. Simulated TPD spectra for HiPIMS samples 6 (10 μm, 0.8 at% D) and 56 (1 μm, 30 at% D). Initial diffusion-trapping parameters are taken from [6]. Detailed description of cases is given in the text.

spectra of HiPIMS samples are the following: (i) low content layers show outgassing peaks at 700–900 K; (ii) these 'high temperature' outgassing peaks are noticeably narrower than those of JET; (iii) high content layers are pre-dominantly outgassing at much lower temperatures with peaks at 500–600 K; (iv) these 'low temperature' peaks are extremely narrow and sharp. Similar sharp release is from for the UCSD sample in figure 1, where it is observed only under specific deposition conditions (e.g. high D_2 partial pressure) [12].

As a starting point for modelling of TPD spectra we use the diffusion-trapping parameters that were proven to describe the outgassing of UCSD samples relatively well (see tables 1 and 2 in [6]). The first two trap energies, about 0.8 V and about 1.0 eV, are also similar to those used for JET samples in [3], where also an additional trap type with 1.4 eV de-trapping energy had to be used. For the JET sample 1/10 shown in figure 1 somewhat different modelling assumptions were used as reported in [5], which will not be discussed here. Figure 2 shows the TPD modelling results for HiPIMS samples 6 and 56. Three examples are shown for sample 6 in blue, red and green (lines with symbols). The first one (blue) corresponds to the case with 1 trap type of 0.8 eV and the trap occupancy of 5%. The profile is significantly broader as compared to the measured spectrum of sample 6. Within the diffusion-trapping model, the most narrow peaks are obtained by switching off the re-trapping processes, which is re-capture of solute population in empty traps during diffusive transport towards the surface. This approach requires at the same time an adjustment of de-trapping energies to higher values to keep the peak positions unchanged. Applying this assumption to sample 6, the TPD peaks become very narrow so that at least 3 trap types with de-trapping energies of 2.1–2.5 eV have to be used to fit the experimental data. An example of the TPD spectra modelled in such a way with 5 trap types is shown in figure 2 (red solid curve). It has to be noted that re-trapping strongly affects the peak position and therefore makes it difficult to fit both, the de-trapping energy and the trap occupancy, without imposing additional constraints on the
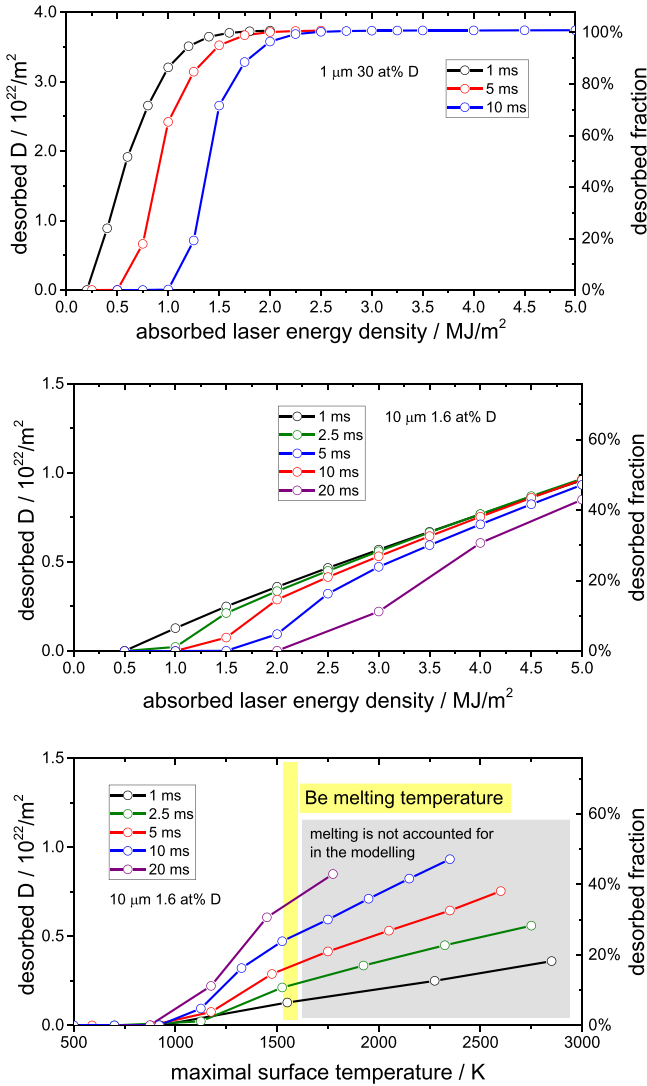
Figure 3. Modelled LID efficiency for a 1 μm thick Be/D layer with 30 at% D content (upper plot) and a 10 μm thick Be/D layer with 1.6 at% D content (middle plot). To be compared with measured LID-QMS data in figure 5 in [7] and in figure 2 in [8]. Modelling assumptions are described in the text. The lower plot shows the LID efficiency for the low D content layer against the surface temperature reached during LID. Each point corresponds to different absorbed laser energy density as in above plots.

system, especially when traps of more than one type are involved. With re-trapping switched off, the trap occupancy does not play any role, so there is somewhat less ambiguity in the model. In the third example shown in figure 2 by green curve there are two trap types assumed. The first trap with 0.86 eV de-trapping energy has 10% occupancy and re-trapping is active. The second trap has 2.07 eV de-trapping energy and there is no re-trapping there. This fit is better at the tails but worse at the peak center that actually contributes the most to the retention. Sample 56 shows a single very narrow low temperature peak at around 500 K. Applying the same assumption of no re-trapping, the peak position can be roughly fitted by the de-trapping energy of about 1.5 eV (solid magenta line in figure 2), keeping all other parameters unchanged (diffusion, de-trapping frequency, recombination

coefficient). The simulated peak remains nevertheless significantly broader than the measured one and has a substantially different shape. It can be speculated a lot, which mechanisms underlie such release behaviour. Similar sharp low temperature peaks were measured for ion implanted crystalline Be [13], as well as for some UCSD samples deposited under specific conditions (e.g. high D_2 partial pressure) [12]. Založnik *et al* were able to explain such release by modelling accounting for de-composition of beryllium deuteride [11]. Presence of beryllium deuteride in ion implanted crystalline Be was detected on one particular sample reported in [14], and despite attempts could not be reproduced since then. Indication of presence of deuteride in Be/D co-deposited layers was given by XPS measurements in [15]. From the modelling point of view, several approaches can be considered to produce similar very sharp release peaks, which rely, however, on ad hoc assumptions. One approach is to assume delayed switching off of re-trapping that can be associated, for example, with trap annealing. In this case the release starts normally, but is then sped up due to reduction or vanishing of re-trapping. Similar effect is achieved assuming a collective release of deuterium (e.g. collapse of a bubble) at a given temperature. Formation of bubbles and interconnected voids has been reported in the literature for D ion implanted polycristalline Be [16, 17]. Another approach is to assume pure surface recombination limited desorption with a step-like reduction of the recombination energy barrier, e.g. due to surface saturation with deuterium. Such a reduction has been predicted recently by DFT-NEB calculations for tungsten [18]. Similar results have been presented earlier for beryllium [19]. An example of simulation using this approach is shown in figure 2 by the dashed magenta line. Here we assumed the initial recombination coefficient in the form

$$K_r \left[\frac{m^4}{s} \right] = 3.4 \cdot 10^{-25} \exp\left(-\frac{1.4 \, [\text{eV}]}{k_B T} \right)$$

and a smooth reduction of the energy barrier from 1.4 to 1.05 eV. The onset time and smoothness of the transition was set manually to fit the peak position.

3. Modelling of laser induced desorption

For the modelling of the LID process we consider two cases corresponding to the experimental studies described in [7] and [8]. For the case of low D content (sample 6) we assume only 'high temperature' contribution to the retention, while for the case of the high D content (sample 56) we assume only the 'low temperature' contribution to the retention, that actually reflects the experimental data shown in figure 1. Taking into account the complexity of parameter adjustment for modelling of TDS spectra and issues with adhesion of layers during TDS and LID experiments, the presented modelling of the LID process has a rather qualitative character.

We choose the simple modelling cases that describe the positions of the respective release peaks and neglect the sharp nature of the low temperature peak. Namely we use the

approximation of no re-trapping with respectively high trap energies for the 'high temperature' peaks case (5 traps, 2.1–2.5 eV) and lower trap energies for the 'low temperature' peak case (1 trap, 1.5 eV), as described in the previous section on modelling of TDS spectra. The temperature evolution is calculated for given values of the absorbed laser density, matching the experimental time evolution of the laser intensity and the estimated maximal surface temperature reached during LID. Results of respective simulations for the two cases described above, varying the laser pulse duration and the absorbed laser power density, are presented in figure 3 as equivalent to experimental data shown in figure 5 in [7] and in figure 2 in [8].

For the case of high D content when the 'low temperature' release dominates in TDS (upper plot in figure 3), modelling results generally agree with the experimental data: a complete release is observed for all laser pulse durations for the absorbed laser energy density above 1.5–2 MJ m^{-2}. Threshold laser energy densities for different pulse duration match. Significant release is observed for the maximal achieved surface temperatures below Be melting.

Quite an opposite is observed for the case of low D content dominated by the 'high temperature' release in TDS (middle plot in figure 3). Here, contrary to the experiment, only up to 50% of the D content is released at the absorbed energy density of 5 MJ m^{-2}, which leads to surface temperatures far beyond the Be melting threshold (lower plot in figure 3). Only 10%–30% of the retained D amount is released at absorbed energy densities corresponding to near melting threshold surface temperatures, and this is in agreement with the experimental data (figure 2 in [8]). Threshold laser energy densities for different pulse duration also match. Therefore, modelling indirectly confirms that the major release in the LID experiments for such low content layers occurs only with the onset of local melting.

4. Conclusions

Modelling of TPD and LID experiments with co-deposited Be/D layers produced by the HiPIMS technique was presented. Experimental spectra were compared with those of UCSD and JET samples. HiPIMS spectra show narrower peaks that cannot be modelled with diffusion-trapping parameters that were applied for modelling of UCSD and JET samples.

LID modelling was performed under the assumption of no-re-trapping. The trap energies were fitted to match the experimental peak temperatures. Modelling results reproduce experimental threshold laser energy densities for D release at different pulse durations. There is qualitative agreement with experimental observations with respect to full or partial outgassing for sample temperatures below the melting threshold during laser heating. Modelling indirectly confirms that the major release in the LID experiments for low D content HiPIIMS layers, characterized by high de-trapping energies, occurs only with the onset of local melting.

With respect to extrapolations to LID efficiency in ITER, modelling and experiments suggest that high D content layers (with low de-trapping energies) can be successfully and completely outgassed in a single laser pulse without layer melting, while low D content layers can be outgassed only to less than 50% without layer melting. Experimental data for low D content layers suggests, however, that almost complete outgassing can be achieved if melting of the surface can be tolerated in ITER. These extrapolations have so far a low level of confidence, in particular due to different behavior of HiPIMS layers compared to layers obtained at JET. Further analyses of reactor-relevant layers from JET, especially LID studies on such layers, are required to assess whether HiPIMS samples can be used as representative model systems for ITER.

ORCID iDs

D Matveev ⬤ https://orcid.org/0000-0001-6129-8427
M Zlobinski ⬤ https://orcid.org/0000-0002-1395-7165
G De Temmerman ⬤ https://orcid.org/0000-0002-4173-0961
C Linsmeier ⬤ https://orcid.org/0000-0003-0404-7191

References

[1] Widdowson A *et al* 2017 *Nucl. Fusion* **57** 8
[2] Schmid K *et al* 2015 *Nucl. Fusion* **55** 053015
[3] Temmerman G D *et al* 2017 *Nucl. Mater. Energy* **12** 267–72
[4] Heinola K *et al* 2017 *Nucl. Fusion* **57** 086024
[5] Likonen J *et al* 2019 *Nucl. Mater. Energy* **19** 166–78
[6] Baldwin M J *et al* 2014 *Nucl. Fusion* **54** 073005
[7] Zlobinski M *et al* 2019 *Nucl. Mater. Energy* **19** 503–9
[8] Zlobinski M *et al* 2020 *Phys. Scr.* accepted (https://doi.org/10.1088/1402-4896/ab5ea1)
[9] Dinca P *et al* 2017 *Surf. Coat. Technol.* **321** 397–402
[10] Matveev D *et al* 2018 *Nucl. Instrum. Methods* B **430** 23
[11] Založnik A *et al* 2019 *Nucl. Fusion* **59** 126027
[12] Baldwin M *et al* 2020 *Phys. Scr.* accepted (https://doi.org/10.1088/1402-4896/ab41a3)
[13] Eichler M *et al* 2019 *Nucl. Mater. Energy* **19** 440–4
[14] Pardanaud C *et al* 2015 *J. Phys.: Condens. Matter* **27** 475401
[15] Doerner R P *et al* 2009 *J. Nucl. Mater.* **390–391** 681–4
[16] Chernikov V N *et al* 1996 *J. Nucl. Mater.* **233–237** 806–64
[17] Yoshida N *et al* 1996 *J. Nucl. Mater.* **233–237** 874–9
[18] Ajmalghan M *et al* 2019 *Nucl. Fusion* **59** 106022
[19] Stihl C and Vladimirov P V 2016 *Nucl. Mater. Energy* **9** 547–53